Tunnel magnetoresistance in epitaxially grown magnetic tunnel junctions using Heusler alloy electrode and MgO barrier

S. Tsunegi[1], Y. Sakuraba[2], M. Oogane[1], N. D. Telling[3, 4], L. R. Shelford[5], E. Arenholz[6], G. van der Laan[5, 7], R. J. Hicken[5], K. Takanashi[2] and Y. Ando[1]

[1]Department of Applied Physics, Graduate School of Engineering, Tohoku University, Aoba-yama 6-6-05, Sendai 980-8579, Japan

[2]Institute for Materials Research, Tohoku University, 2-1-1 Katahira, Aoba-ku, Sendai 980-8577, Japan

[3]School of Earth, Atmospheric and Environmental Science, University of Manchester, Oxford Road, Manchester M13 9P, United Kingdom

[4]Magnetic Spectroscopy Group, STFC Daresbury Laboratory, Warrington WA4 4AD, United Kingdom

[5]School of Physics, University of Exeter, Stocker Road, Exeter EX4 4QL, United Kingdom

[6]Advanced Light Source, Lawrence Berkeley National Laboratory, Berkeley, California 94720, USA

[7]Diamond Light Source, Chilton, Didcot OX11 0DE, United Kingdom

Abstract

Epitaxially grown magnetic tunnel junctions (MTJs) with a stacking structure of Co_2MnSi/MgO/CoFe were fabricated. Their tunnel magneto-resistance (TMR) effects were investigated. The TMR ratio and tunnelling conductance characteristics of MTJs were considerably different between those with an MgO barrier prepared using sputtering (SP-MTJ) and those prepared using EB evaporation (EB-MTJ). The EB-MTJ exhibited the very large TMR ratio of 217% at room temperature and 753% at 2 K. The bias voltage dependence of the tunnelling conductance in the parallel magnetic configuration for the EB-MTJ suggests that the observed large TMR ratio at RT results from the coherent tunnelling process through the crystalline MgO barrier. The tunnelling conductance in the anti-parallel magnetic configuration suggests that the large temperature dependence of the TMR ratio results from the inelastic spin-flip tunnelling process.

1. Introduction

Magnetic tunnel junctions (MTJs) are key devices in the spintronics field because MTJs are fundamental devices used for magnetic random access memory (MRAM), magnetic sensors and innovative spintronics devices, such as spin-transistors and microwave generators. High spin polarization materials are necessary to increase TMR effects and to enhance spintronics device performance. Ideal high spin polarization materials are half metallic ferromagnets (HMFs)[1, 2], which have a band gap at the Fermi level for one spin band. Several full-Heusler alloy compounds

such as $Co_2Mn(Al, Si)$, Co_2MnGe, $Co_2(Cr, Fe)Al$ are predicted to be HMFs theoretically[3] if they have the ordered $L2_1$ structure. In addition, some Co-based full-Heusler alloys have a high Curie temperature. Experimentally, some groups have used Heusler alloys as MTJ electrodes with an amorphous Al-oxide barrier[4–8]. We have achieved a large TMR ratio of 159% at 2 K in the optimized MTJ with Co_2MnSi/Al-O/CoFe structure[9]. This result proved the half-metallic property of Co_2MnSi (CMS) experimentally. However, in this MTJ, the large temperature dependence of the TMR ratio was a serious problem; the TMR ratio at room temperature (RT) was only 70%.

According to Julliere's model[10], for MTJs with an amorphous tunnelling barrier the TMR ratio depends only on the density of states (DOS) at the Fermi level of the ferromagnetic electrodes. On the other hand, in MTJs with a (001)-oriented crystalline MgO tunnelling barrier and bcc-structured ferromagnetic electrodes, Δ1-band selective coherent tunnelling occurs and enhances the TMR ratio drastically compared with an MTJ with an amorphous barrier[10, 11]. Some groups have reported very large TMR ratios greater than 200% at RT in the MTJs with Fe, CoFeB electrodes and a MgO barrier[12, 13]. Recently, some groups have attempted to use Heusler alloy electrodes and a crystalline MgO barrier together in the MTJs. Yamamoto et al. observed oscillation of TMR ratio against the MgO barrier thickness[14]; Tezuka et al. observed TMR ratio over 200% at RT[15]. These results are apparently related to the coherent tunnelling process through the crystalline MgO barrier. In addition, Miura et al. suggested theoretically that coherent tunnelling can enhance the TMR ratio in a MTJ with Heusler alloy electrodes and a MgO

barrier[16].

This review article presents our recent work on TMR effects in high-quality epitaxially grown Co_2MnSi/MgO/CoFe MTJ. Particularly, we note that the CMS/MgO interface structure is important for realizing a large TMR effect, and that the interface structure is sensitive to the electrode fabrication conditions and the preparation method for the MgO barrier. Furthermore, we discuss the coherent tunnelling process and inelastic tunnelling process, considering results of the tunnelling conductance measurement.

2. Experimental procedure

The (001)-oriented epitaxial Co_2MnSi bottom electrode was grown on Cr-buffered MgO (001) substrate at ambient temperature by inductively coupled plasma (ICP)-assisted magnetron sputtering. The deposition pressure was 0.1 Pa and the rate was about 0.03 nm/s. The film was subsequently annealed at 500°C to reduce site-disorder and create highly oriented film. To obtain the stoichiometric film composition, we used a composition-adjusted Co-Mn-Si alloy sputtering target (Co, 43.7%; Mn, 27.95%; Si, 28.35%). The crystallographic structure and surface morphology of the bottom CMS were observed using x-ray diffraction (XRD) with Cu K_α radiation; surface roughness was verified using atomic force microscopy (AFM). We measured magnetization curves using a vibrating sample magnetometer (VSM) and a superconducting quantum interference device (SQUID) magnetometer. Film compositions were examined using inductively coupled plasma (ICP) analysis. X-ray absorption spectroscopy measurements were

performed on beamline 6.3.1 at the Advanced Light Source, Lawrence Berkeley National Laboratory, using total electron yield detection.

The result of the XRD θ/2θ measurement for the bottom electrode showed only the (002) Cr peak and (002) and (004) CMS peaks except for the peaks from MgO substrates, indicating perfect (001)-orientation of the CMS. Additionally, we confirmed epitaxial growth and highly $L2_1$ order of CMS film from the ϕ-scan measurement. The long range order parameters S_{B2} and S_{L21} are, respectively, ca. 1.0 and ca. 0.8. Results of AFM measurements showed that the surface of the CMS was very smooth: R_a and peak–valley (*P*-*V*) values were, respectively, about 0.2 nm and 2.0 nm. The magnetization of CMS was almost 5 μ_B, as predicted by the Slater–Pauling curve for Heusler alloys. These results show that the prepared CMS thin film is suitable for the bottom electrode of the MTJ[17].

The epitaxially grown MTJs with the structure of MgO(001)-subs/Cr (40 nm)/Co_2MnSi (30 nm)/MgO (t_{MgO})/CoFe (5 nm)/IrMn (10 nm)/Ta (5 nm) were prepared. The all-metal thin films were deposited using a direct-magnetron sputtering system. The MgO barrier was formed using a direct-magnetron sputtering and electron beam (EB) evaporation system. We describe the MTJs with a sputtered MgO barrier as SP-MTJ and the EB-evaporated MgO barrier as EB-MTJ. The Ar pressure was 0.1 Pa in the MgO sputtering and the deposition rate was about 0.008 nm/s. The pressure during evaporation was about 2×10^{-6} Pa and typical evaporation rate was 0.01 nm/s. The MTJ films were patterned into 8 × 8 – 90 × 90 μm^2 elements using photolithography combined with Ar ion etching. After micro-fabrication, the MTJs were annealed under a high vacuum and

an external magnetic field of 1T. We measured TMR effects using a standard dc four-probe method at a bias voltage of 1 mV and differential conductance using an ac-lock-in technique.

3. TMR effects

Figures 1(a) and 1(b) depict cross-sectional high-resolution transmission electron micrograph (TEM) images along the [1–10] direction of the CMS film for the SP-MTJ annealed at 400°C and the EB-MTJ annealed at 475°C, respectively. Both TEM images reveal epitaxial growth from the bottom Cr/CMS electrode to the CoFe top electrode. However, for the SP-MTJ, a disarray structure was observed at the CMS/MgO interface. On the other hand, for the EB-MTJ, extremely smooth and abrupt interfaces were formed, as shown in the TEM image.

X-ray absorption (XA) measurements were used to investigate the CMS/MgO interface for both CMS/MgO multilayers prepared using direct sputtering and the EB-evaporation. MgO thickness on both prepared samples was 2 nm. The Co $L_{2,3}$ XA spectra are shown in Figure 2. For the CMS/MgO layer prepared using sputtering, the shoulder feature just after the main L_3 absorption peak that originates from $L2_1$ ordering of the CMS [18] was very weak, indicating the disarray pertaining at the CMS/MgO interface. On the other hand, for the CMS/MgO layer prepared using EB-evaporation, this shoulder was clearly visible, indicating that the CMS at the MgO interface has an $L2_1$ ordered structure[18]. The Mn $L_{2,3}$ XA spectra are shown in Figure 3. The XA peaks at the Mn $L_{2,3}$ absorption edge were also measured to investigate the oxidation of the CMS at the MgO barrier interface. For the CMS/MgO layer prepared using sputtering, additional

features around the L_3 absorption peak were clearly visible indicating that oxidation of Mn atoms occurred. For the CMS/MgO layer prepared using EB-evaporation, the Mn absorption spectrum does not contain this additional structure, suggesting that a clean CMS/MgO interface is formed[18]. We note that the XAS results are consistent with the HR-TEM images.

Figure 4 portrays the annealing temperature (T_a) dependence of the TMR ratio at RT and the MR curves on the each MTJs. The TMR ratio increased with increasing annealing temperature. Previous investigations have indicated that the improvement of TMR ratio by annealing results from improvements of both crystallinity and (001)-orientation of the MgO barrier at the electrode/barrier interface[19]. Furthermore, the degradation of TMR by high-temperature annealing was caused by atomic diffusion, especially of Mn atom in the pinning layer[19]. The TMR ratio of the as-deposited EB-MTJ is almost the same as that of the as-deposited SP-MTJ even though the anti-parallel magnetic configuration in the EB-MTJ is poor. This means that the quality of MgO layer in the EB-MTJ should be better than that of the SP-MTJ. For the SP-MTJ, the TMR ratio showed a maximum of 80% at T_a=375°C, this TMR ratio was rather smaller than those of the MTJs with CoFeB electrodes and a MgO barrier, reported previously[19]. In addition, the $R\times A$ value is almost 10^8 Ω μm^2 and larger than the EB-MTJ (~10^5 Ω μm^2) and the previous CoFeB/MgO/CoFeB-MTJ (~10^5 Ω μm^2), although the MgO barrier thickness was same[19]. Both the small TMR ratio and the large $R\times A$ value for the SP-MTJ are thought to result from tunnelling electron scattering at the MgO barrier interface.

On the other hand, the EB-MTJ showed a maximum TMR ratio of 217% at T_a=475°C. This

TMR ratio is much larger than that of the SP-MTJ; it is comparable to that of the CoFeB/MgO/CoFeB-MTJ reported previously. Both good crystallinity and high (001)-orientation of the MgO barrier can promote the coherent tunnelling process through the Δ1 band of the CMS. We note that the reduction of tunnel resistance by the coherent tunnelling process enhances the TMR effect at RT, compared with the SP-MTJ with the worse MgO interface. In addition, the thermal endurance of the fabricated MTJ is better than those of the spin-valve type MTJs with other ferromagnetic electrodes[19], such as CoFeB. This good thermal endurance is a feature of MTJs with crystalline Heusler alloy electrodes.

Figure 5 depicts the temperature dependence of the TMR ratio both for the SP-MTJ and EB-MTJ exhibited a maximum TMR ratio at RT. As a reference, data for both the CoFeB/MgO/CoFeB prepared using EB-evaporation are also shown in figure 5. The TMR curves measured at various temperatures on the SP-MTJ and the EB-MTJ are shown in figure 5. The TMR ratio drastically increased with decreasing temperature for both MTJs. We observed the large TMR ratio of 330% for the SP-MTJ and very large TMR ratio of 753% for the EB-MTJ at 2 K. The TMR ratio of 753% at 2 K is high in the MTJs using Heusler alloy electrodes and much larger than those of CoFeB/MgO/CoFeB-MTJ (400% at 2 K). This result reveals that the half-metallicity of the CMS can be realized not only in the MTJ with an amorphous Al-oxide barrier, as previously reported, but in the MTJ with a crystalline MgO barrier. However, contrary to our expectation, the temperature dependence of TMR ratio is strong, even in the MTJ with MgO barrier.

4. Tunnelling conductance characteristics

The bias voltage dependence of the differential conductance (*G*-*V*) curves at 10 K was measured for both parallel (G_P) and anti-parallel (G_{AP}) magnetic configurations to investigate the tunnelling process mechanism. The G_P and G_{AP} curves for the SP-MTJ are portrayed respectively in figures 6(a) and 6(b). In figure 6(a), the previously reported G_P-*V* curve for the CMS/Al-oxide/CoFe-MTJ is shown also. For the CMS/Al-oxide/CoFe-MTJ, the G_P was definitely asymmetric with respect to the sign of bias voltage and the crucial rise of G_P was observed at the bias voltage of -10 mV and 350 mV. We suggested that the values of -10 mV and 350 mV correspond to the bottom edge of the conduction band and the top edge of the valence band, respectively, for the half-metallic band gap of the CMS electrode. Furthermore, we inferred that the small energy separation between the Fermi level and the edge of the half-metallic gap is the origin of the large temperature dependence of the TMR ratio for the MTJ with Al-oxide barrier[20]. For the SP-MTJ, the G_P characteristic resembled that of the MTJ with Al-oxide barrier, although the crucial rise of G_P at negative bias voltage was suppressed slightly. That fact indicates that the coherent tunnelling process does not occur in the SP-MTJ. In figure 6(b), the G_{AP}-*V* curves for both CMS/Al-oxide/CoFe-MTJ and CoFeB/MgO/CoFeB-MTJ are shown together. The G_{AP} exhibited a crucial rise at the low bias voltage for all MTJs, called the zero-bias anomaly. However, for CMS/MgO/CoFe-MTJ, the G_{AP} increased more significantly at lower bias than those of other MTJs. The zero-bias anomaly of G_{AP} originates from inelastic tunnelling processes

and two possible explanations exist for the large inelastic tunnelling probability in the MTJs with CMS electrodes; magnon excitations attributable to the low Curie temperature at the CMS surface and magnetic impurity scatterings caused by some Mn and Si oxides[13,14]. The large zero-bias anomaly for the SP-MTJ is considered to result mainly from impurities of Mn or Si-oxides at the CMS/MgO interface, considering the results of XAS measurements.

Figure 7(a) shows the G_P-V curve measured at both RT and 10K for the EB-MTJ annealed at T_a = 475°C. For comparison, the G_P for the CMS/Al-oxide/CoFe-MTJ is also shown. The G_P-V curve of the CMS/Al-oxide/CoFe-MTJ changes between RT and 10 K because of the thermal broadening of the Fermi level, particularly at the low bias voltage. On the other hand, for EB-MTJ, the shape of G_P-V curve was almost identical between RT and 10 K. Furthermore, the crucial rise of G_P at the negative bias voltage, which is the origin of the large temperature dependence of TMR ratio for the MTJ with Al-oxide barrier[21], seems to be suppressed at both RT and LT. Therefore, the origin of the large temperature dependence of TMR ratio for the EB-MTJ is thought to be different from that of the CMS/Al-oxide/CoFe-MTJ. Figure 7(b) shows G_P curves for the EB-MTJ annealed at various T_a. For comparison, the G_P curve for the CoFeB/MgO/CoFeB-MTJ is also shown. The crucial rise of the G_p in the negative bias voltage is suppressed by increasing T_a. In addition, the dip structure observed at ±400 mV is enhanced by increasing T_a; this dip structure resembles that for the CoFeB/MgO/CoFeB-MTJ[21, 22]. We infer that this dip structure is related to the coherent tunnelling process through the crystalline MgO barrier and that this coherent tunnelling plays an important role in realizing the large TMR effect.

Figure 8 shows G_{AP}-V curves measured at both RT and 10 K for the EB-MTJ annealed at T_a = 475°C. The G_{AP} at 10 K increased sharply at low bias voltage compared with the G_{AP} at RT. This large zero-bias anomaly at 10 K for the EB-MTJ is thought to result mainly from the inelastic tunnelling process[23] caused by magnon excitation because impurities[24] such as Mn and Si oxides were not found (as inferred from the XAS results described previously). Furthermore, theoretically, the exchange interaction energy of the CMS at the CMS/MgO interface is small, indicating that the magnon can be excited easily[25]. At RT, the zero-bias anomaly of the G_{AP} almost disappeared because these inelastic tunnelling processes are stimulated by thermal excitation energy. Therefore, we suggested that the inelastic tunnelling process attributable to the magnon excitation can be the dominant reason for the large temperature dependence of the TMR effect for EB-MTJ.

5. Summary

In summary, we have fabricated epitaxially grown Co_2MnSi/MgO/CoFe-MTJs with a MgO barrier prepared using both direct sputtering and EB-evaporation techniques. For the MTJ with a MgO barrier prepared using sputtering, the TMR ratio was comparable to those of the MTJs using an Al-oxide barrier. From HR-TEM images, XA measurements and conductance curves, we found that the CMS/MgO interface has a disarrayed structure and contains oxides. This poorer interface structure is the reason for the low TMR ratio and large resistance for the MTJ with MgO barrier prepared by sputtering. On the other hand, for the MTJ with the MgO barrier prepared

using EB-evaporation, we observed the highest TMR ratio of 753% at 2 K among the MTJs using Heusler alloy electrodes. However, unfortunately, the temperature dependence of TMR ratio remained large. We discussed the origin of the large temperature dependence of the TMR ratio. Results of this study suggest that this problem is attributable to inelastic tunnelling processes because of magnon excitation at the CMS/MgO interface.

Acknowledgements

This study was supported by the "High-Performance Low-Power Consumption Spin Devices and Storage Systems" program under Research and Development for Next-Generation Information Technology by the Ministry of Education, Culture, Sports, Science and Technology of Japan (MEXT). This research was partly conducted at the Laboratory for Nanoelectronics and Spintronics, Research Institute of Electrical Communication, Tohoku University. The Advanced Light Source is supported by the Director, Office of Science, Office of Basic Energy Sciences, of the U.S. Department of Energy under Contract No. DE-AC02-05CH11231.

References

1) Bowen M, Bibes M, Barthelemy A, Contour J-P, Anane A, Lemaıtre Y, and Fert, A 2003 *Appl. Phys. Lett*. **82** 233

2) Schwart K 1986 *J. Phys. F: Met. Phys.* **16** L211–L215

3) Picozzi S, Continenza A and Freeman A J 2002 *Phys. Rev.* B **66** 094421

4) Tanaka C T, Nowak J and Moodera J S 1999 *J. Appl. Phys.* **86** 6239

5) Kämmerer S, Thomas A, Hütten A and Reiss G 2004 *Appl. Phys. Lett.* **85** 79

6) Conca A, Falk S, Jakob G, Jourdan M, Adrian H 2004 *J. Magn. Magn. Mater.*

7) Inomata K, Okamura S, Goto R, Tezuka N 2003 *Jpn. J. Appl. Phys.* **42** L419

8) Kubota H, Nakata J, Oogane M, Ando Y, Sakuma A, Miyazaki T 2004 *Jpn. J. Appl. Phys.* **43** L984

9) Sakuraba Y, Nakata J, Oogane M, Kubota H, Ando Y, Sakuma A and Miyazaki T 2005 *Jpn. J. Appl. Phys.* Part 2 **44** L1100

10) Julliere M 1975 *Phys. Lett.* **54A** 225

11) Butler W H, Zhang X-G, Schulthess T C and MacLaren J M 2001 *Phys. Rev.* B **63** 054416

12) Yuasa S, Nagahama T, Fukushima A, Suzuki Y and Ando K 2004 *Nat. Mater.* **3** 868

13) Lee Y M, Hayakawa J, Ikeda S, Matsukura F and Ohno H 2007 *Appl. Phys. Lett.* **90** 212507

14) Ishikawa T, Hakamata S, Matsuda K, Umemura T and Yamamoto M 2008 *J. Appl. Phys.* **103**

07919

15) Tezuka N, Ikeda N, Sugimoto S, Inomata K 2007 *Jpn. J. Appl. Phys.* Part 2 **46** L454

16) Miura Y, Uchida H, Oba Y, Nagao K and Shirai M 2007 *J. Phys.: Condens. Matter* **19** 365228

17) Oogane M, Sakuraba Y, Nakata J, Kubota H, Ando Y, Sakuma A and Miyazaki T 2006 *J. Phys.* D **39** 834

18) Telling N D, Keatley P S, Van der Laan G, Hicken R J, Arenholz E, Sakuraba Y, Oogane M, Ando Y and Miyazaki T 2006 *Phys. Rev.* B **74** 224439

19) Hayakawa J, Ikeda S, Matsukura F, Takahashi H and Ohno H 2005 *Jpn. J. Appl. Phys.* **44** L587

20) Hayakawa J, Ikeda S, Lee Y M, Matsumura F and Ohno H 2006 *Appl. Phys. Lett.* **89** 232510

21) Sakuraba Y, Kubota H, Miyakoshi T, Oogane M, Ando Y, Sakuma A and Miyazaki T 2006 *Appl. Phys. Lett.* **89** 052508

22) Matsumoto R, Nishioka S, Mizuguchi M, Shiraishi M, Maehara H, Tsunekawa K, Djayaprawira D D, Watanabe N, Otani Y, Nagahama T, Fukushima A, Kubota H, Yuasa S and Suzuki Y 2007 *Solid State Comm.* **143** 574

23) Miao G, Chetry K B, Gupta A, Butler W H, Tsunekawa K, Djayaprawira D D and Xiao G 2006 *J. Appl. Phys.* **99** 08A905

24) Zhang S, Levy P M, Marley A C, Parkin S S 1997 *Phys. Rev. Lett.* **79** 3744

25) Takada I, Inoue J and Itoh H 2008 *J. Magn. Soc. Jpn.* **32** 338

26) Sakuma A, Toga Y, and Tsuchiura H 2009 *J. Appl. Phys.* **105**, 07C910

Figure captions

Figure 1

HR-TEM images of (a) SP-MTJ with T_a = 375°C and (b) EB-MTJ with T_a = 475°C.

Figure 2

The XA spectra of the half SP-MTJ and the half EB-MTJ at the Co $L_{2,3}$ absorption edges. The arrow indicates a shoulder feature associated with an $L2_1$ ordered Heusler film.

Figure3

The XAS spectra of the half SP-MTJ and the half EB-MTJ at the Mn $L_{2,3}$ absorption edges. The arrow indicates a feature typically of MnO formation.

Figure 4

Annealing temperature dependence of the TMR ratio. The MR curves are samples of various annealing temperatures for the SP-MTJs and the EB-MTJs.

Figure 5

Temperature dependence of the TMR ratio for the SP-MTJ with T_a = 375°C and the EB-MTJ with T_a = 475°C. For reference, previously reported MTJ using the Al-oxide barrier and CoFeB/MgO/CoFeB-MTJ are shown together. The MR curves are shown at various temperatures for SP-MTJs and EB-MTJs.

Figure 6

Conductance curves on the SP-MTJ sample. (a) The parallel configuration at 10 K. (b) The anti-parallel configuration at 10 K.

Figure 7

Conductance curves on the sample of the EB-MTJ with the parallel configuration at 10 K. (a) Comparison with the previous MTJ using an Al-O barrier. (b) Dependence of the annealing temperature.

Figure 8

Conductance curves on the sample of the EB-MTJ with the anti-parallel configuration at 10 K and 300 K.

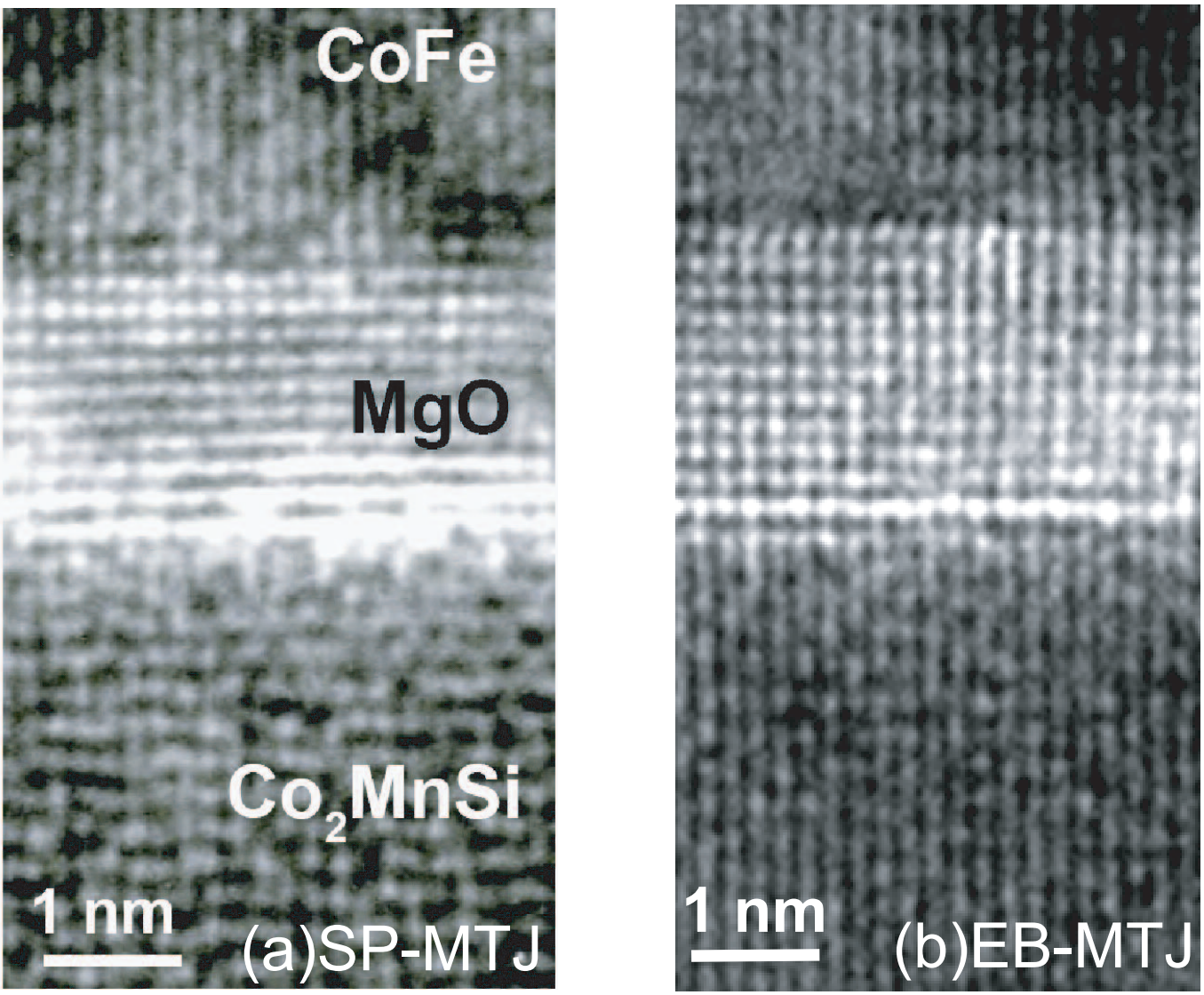

Figure 1 (graph1_final.eps)

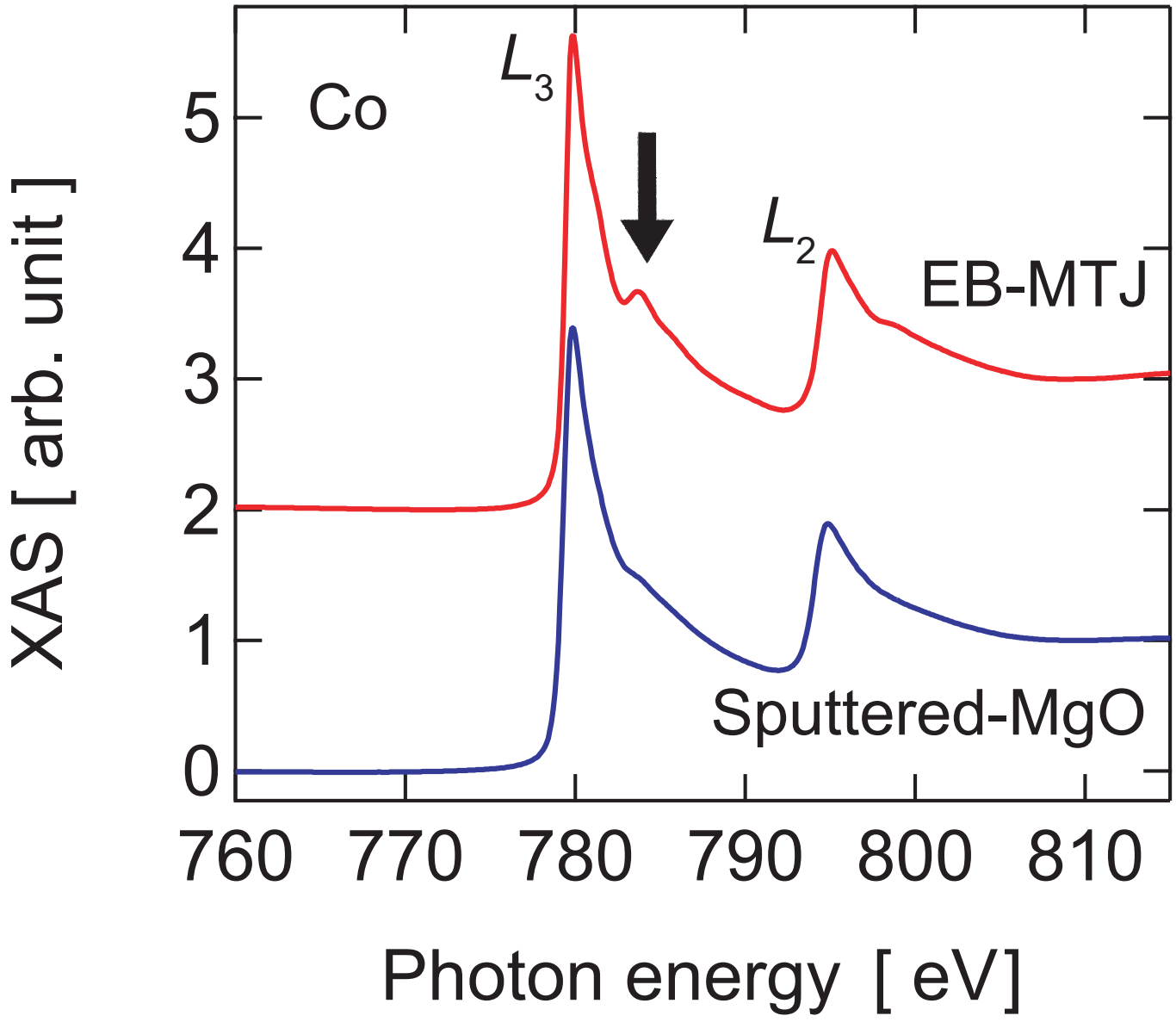

Figure 2 (graph2_final.eps)

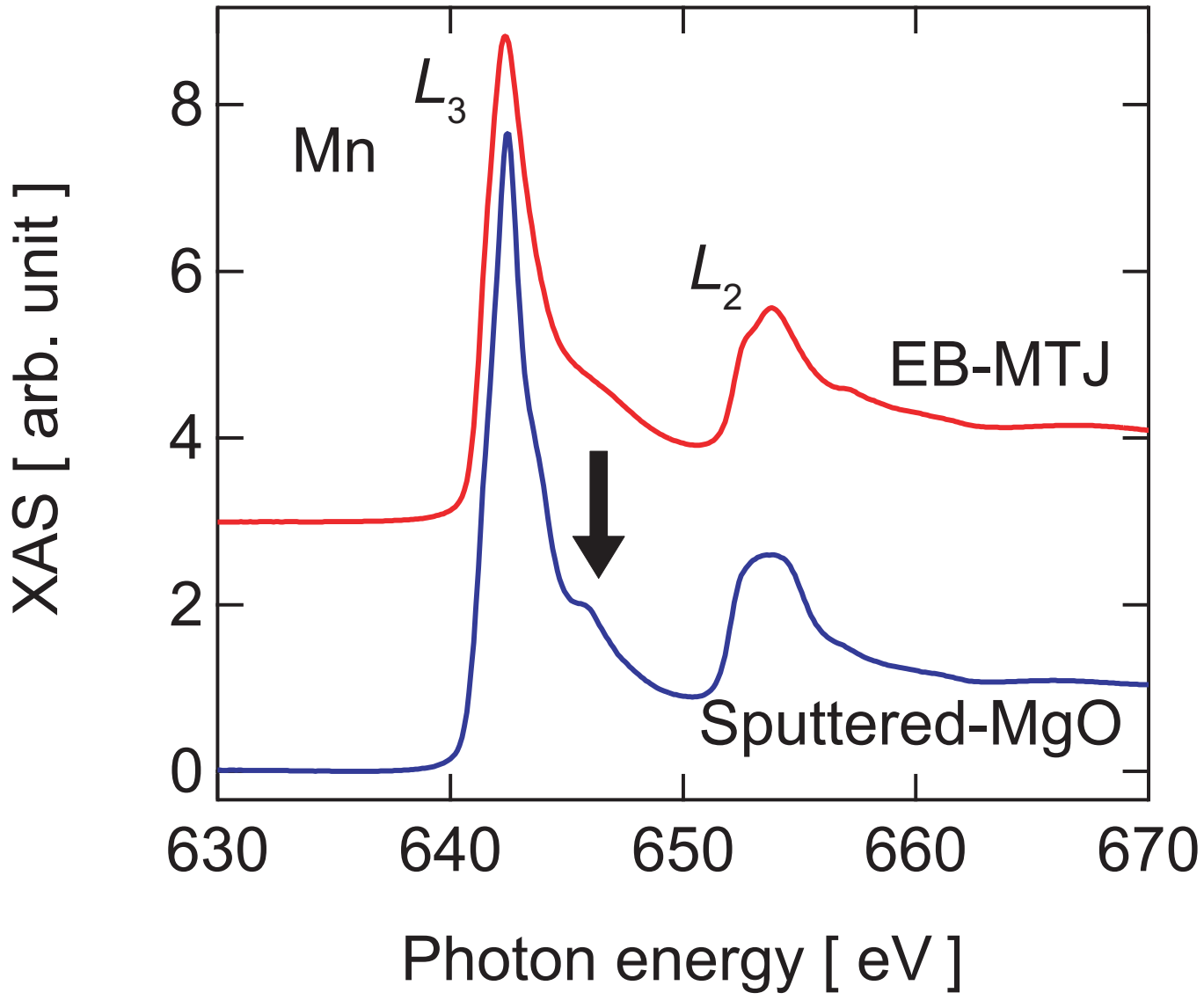

Figure 3 (graph3_final.eps)

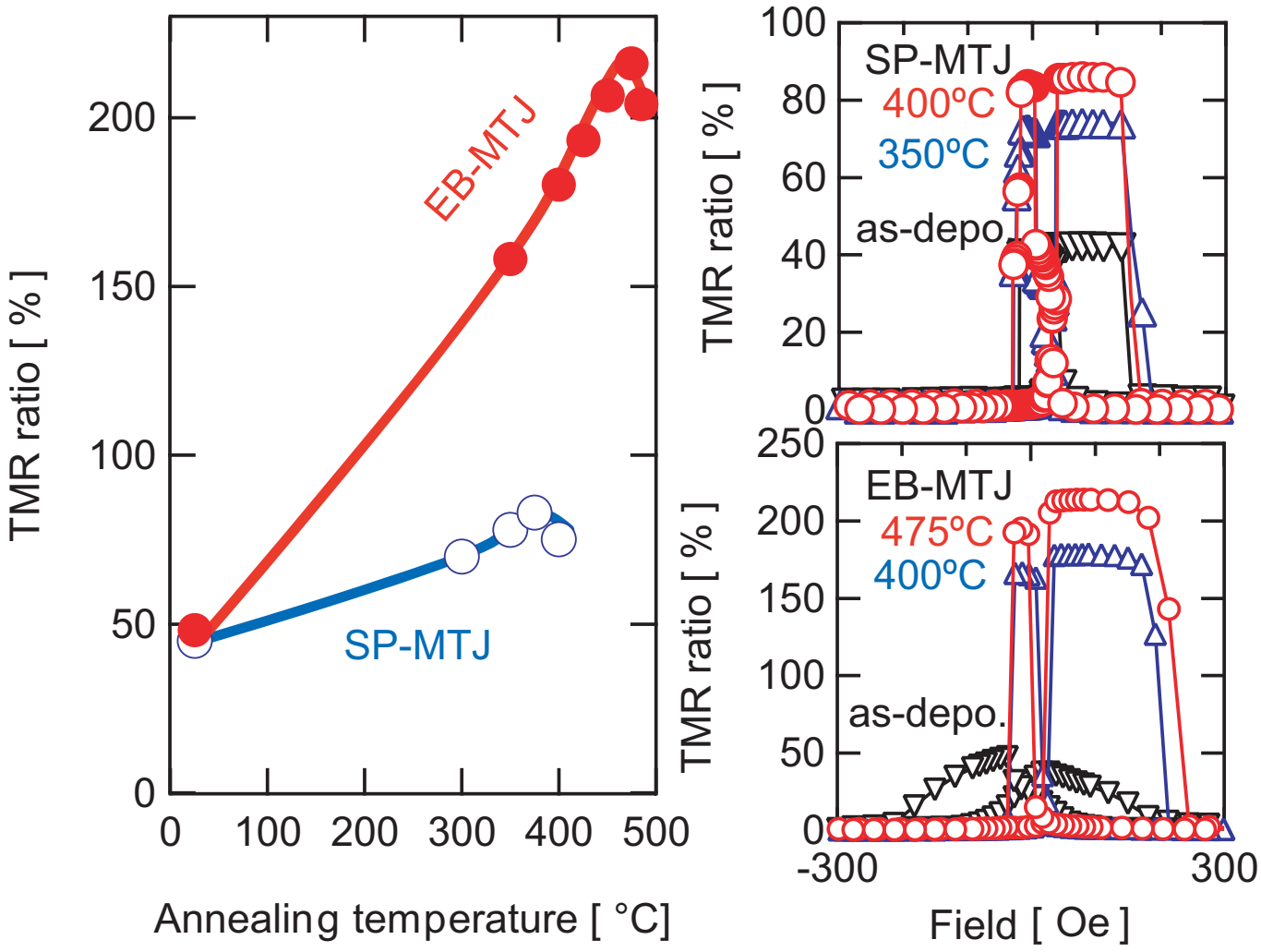

Figure 4 (graph4_final.eps)

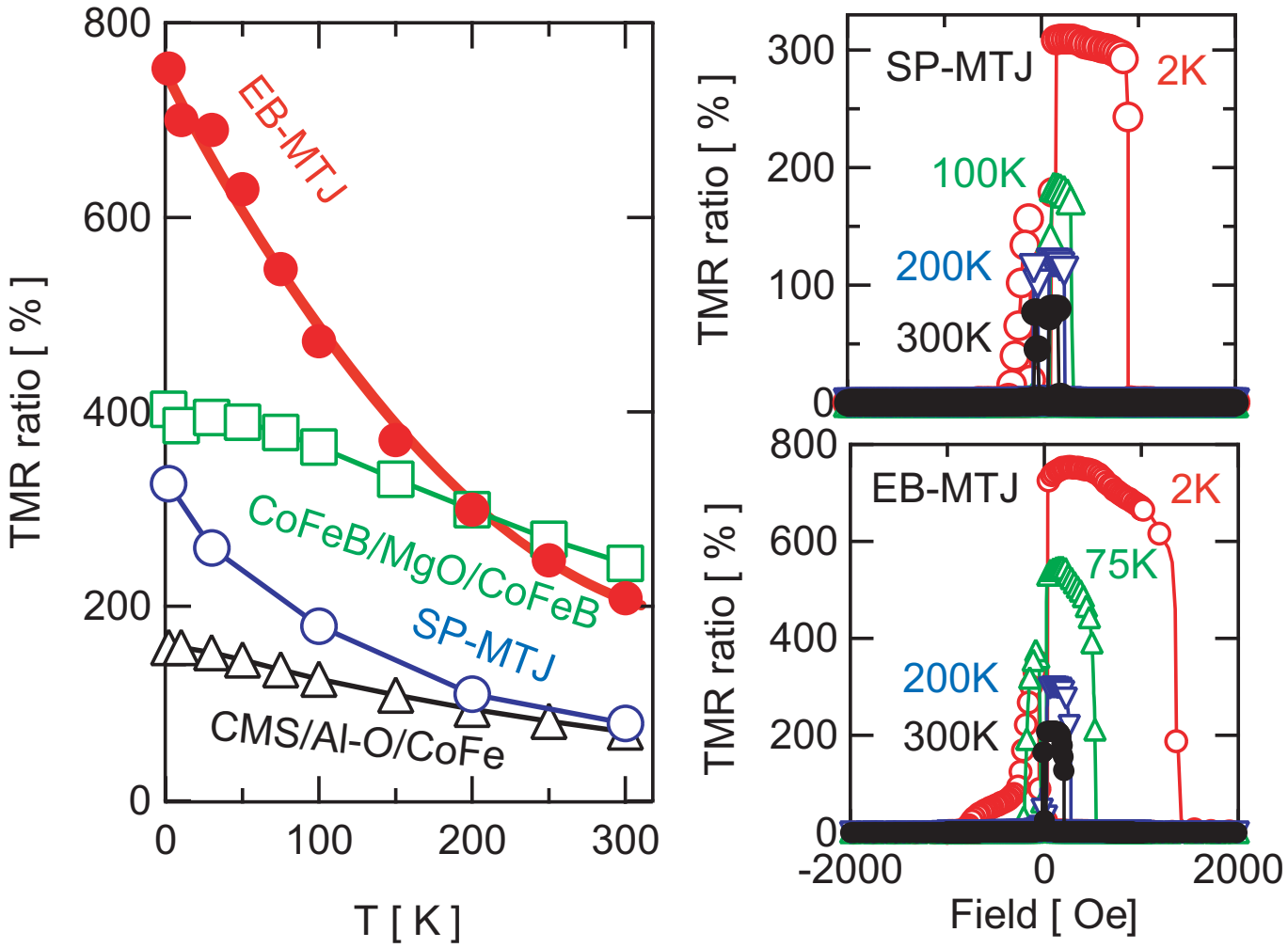

Figure 5 (graph5_final.eps)

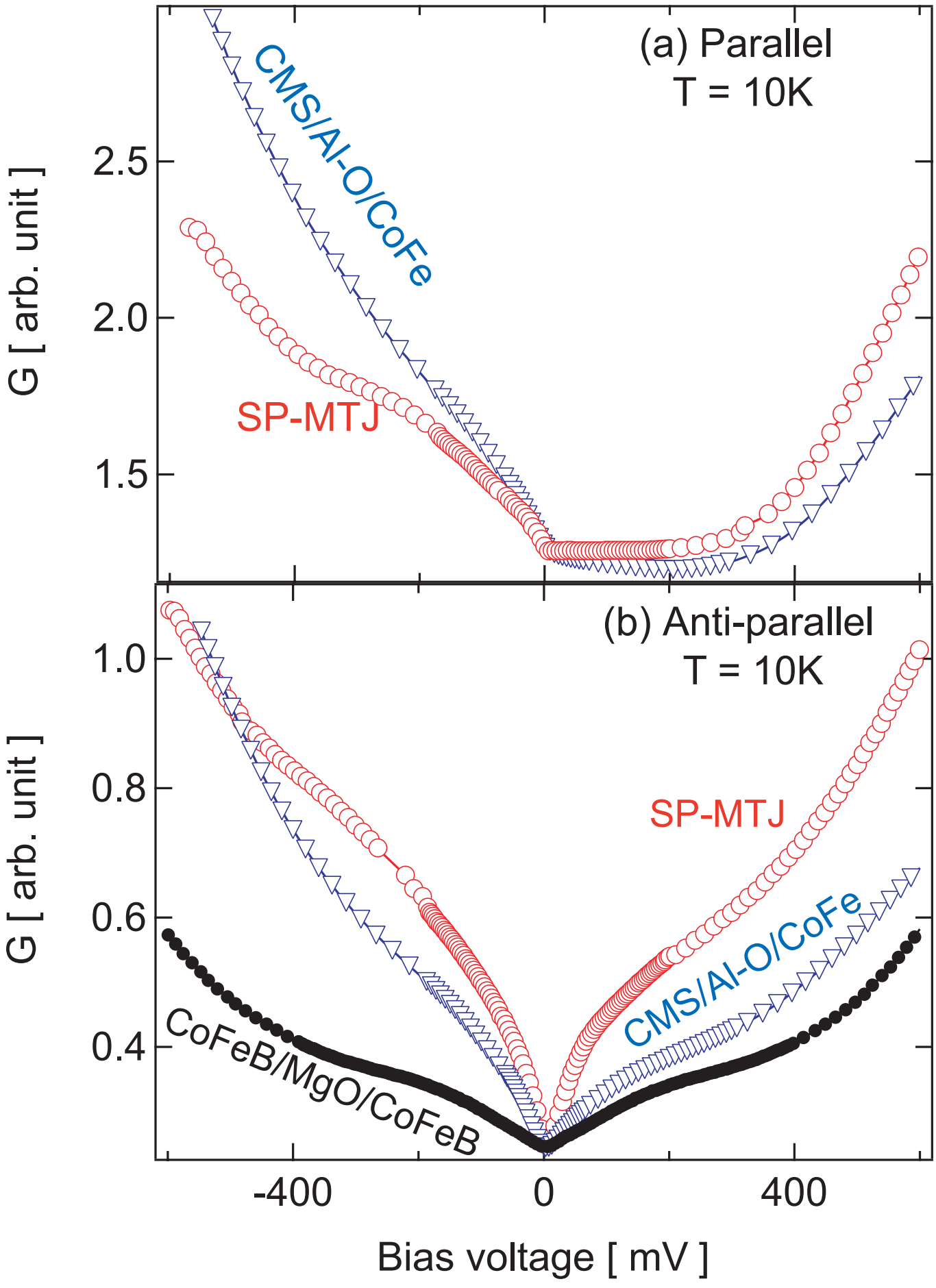

Figure 6 (graph6_final.eps)

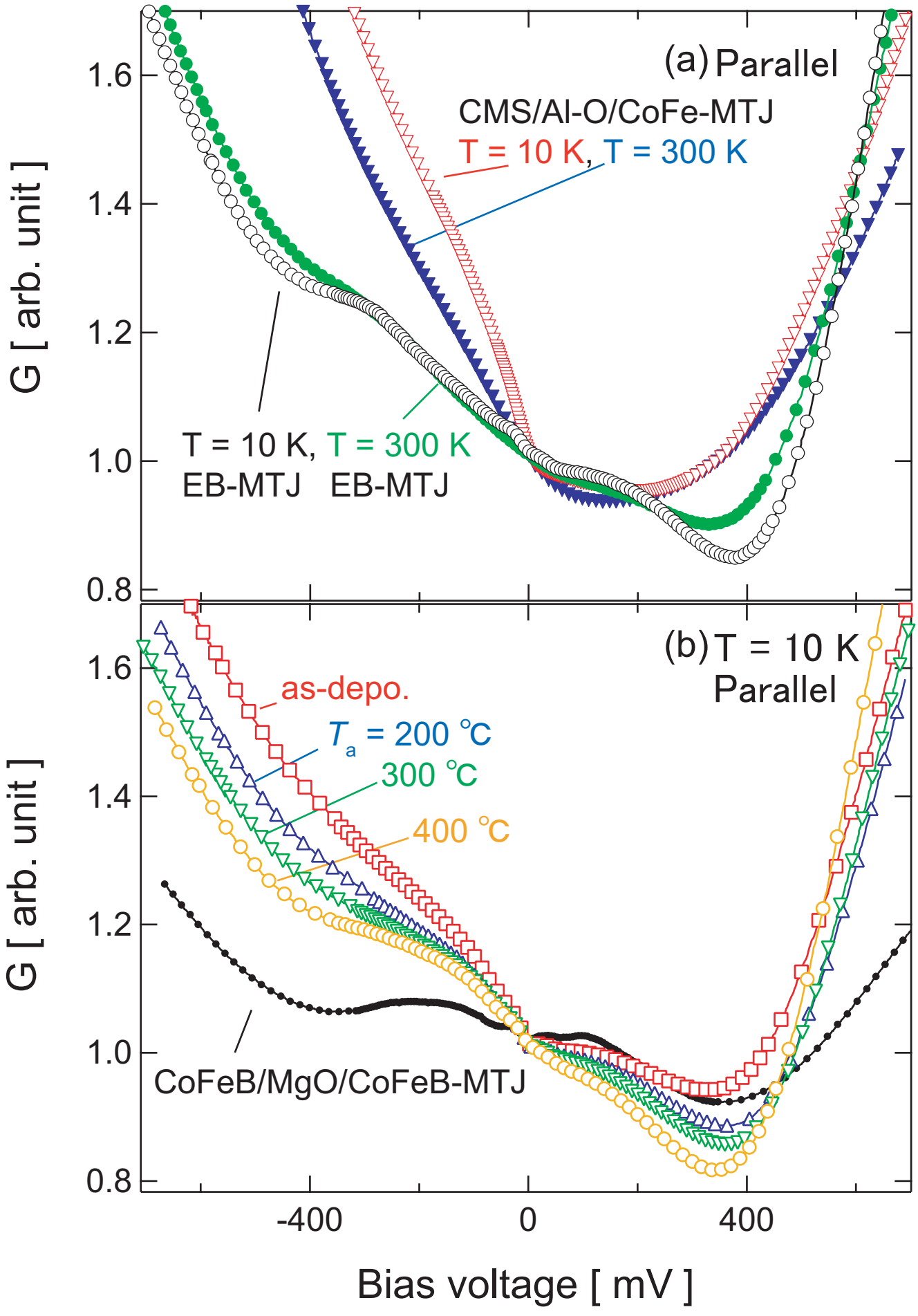

Figure 7 (graph7_final.eps)

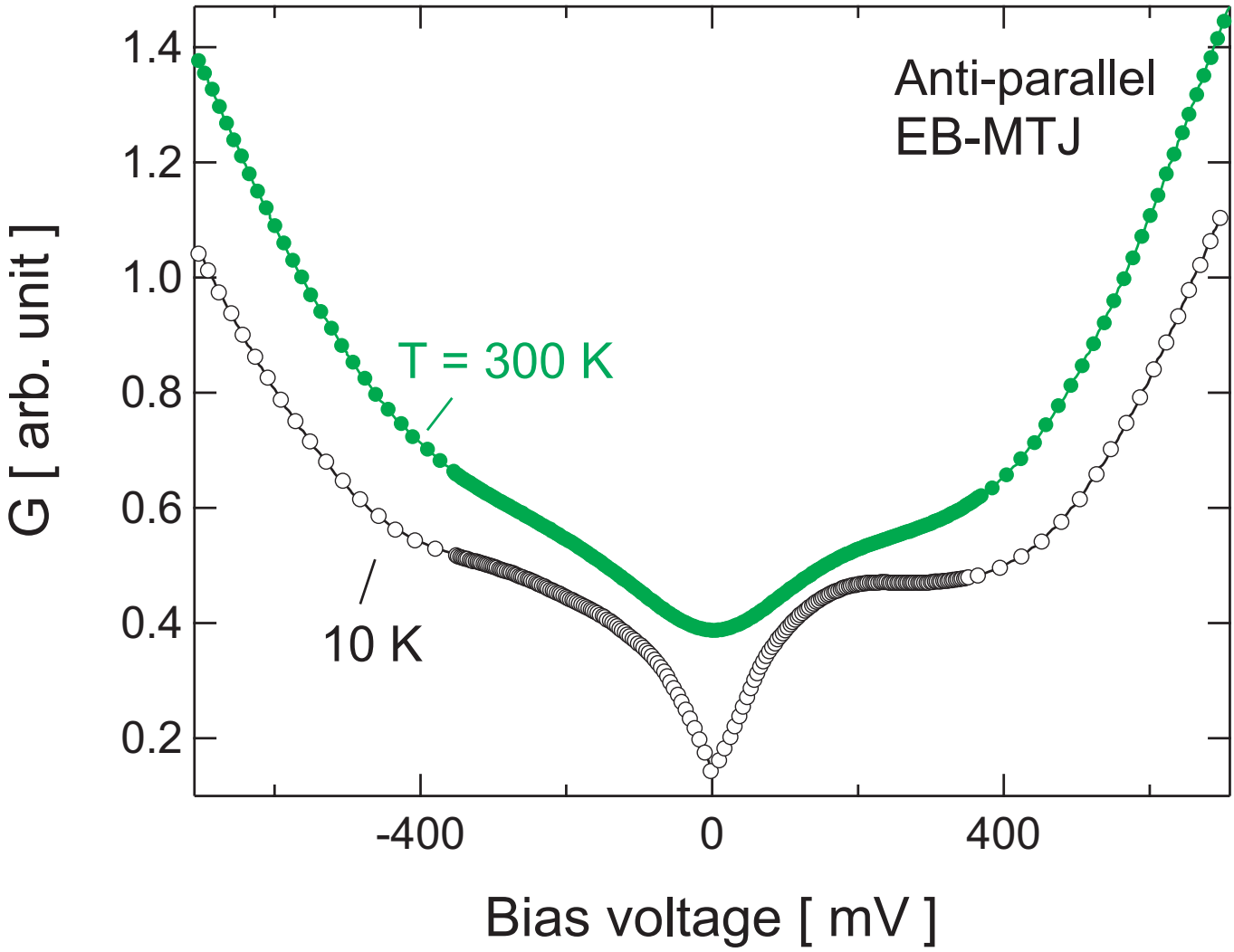

Figure 8 (graph8_final.eps)